FFI RAPPORT

AUTOMATIC DETECTION OF OIL SPILLS BY SAR IMAGES - Dark Spot Detection and Feature Extraction

BREKKE Camillla

FFI/RAPPORT-2005/00893

AUTOMATIC DETECTION OF OIL SPILLS BY SAR IMAGES - Dark Spot Detection and Feature Extraction

BREKKE Camillla

FFI/RAPPORT-2005/00893

FORSVARETS FORSKNINGSINSTITUTT
Norwegian Defence Research Establishment
P O Box 25, NO-2027 Kjeller, Norway

FORSVARETS FORSKNINGSINSTITUTT (FFI)
Norwegian Defence Research Establishment

P O BOX 25
N0-2027 KJELLER, NORWAY

UNCLASSIFIED

SECURITY CLASSIFICATION OF THIS PAGE
(when data entered)

REPORT DOCUMENTATION PAGE

1) PUBL/REPORT NUMBER	2) SECURITY CLASSIFICATION	3) NUMBER OF PAGES
FFI/RAPPORT-2005/00893	UNCLASSIFIED	32
1a) PROJECT REFERENCE	**2a) DECLASSIFICATION/DOWNGRADING SCHEDULE**	
FFI-II/887/913	-	

4) TITLE

AUTOMATIC DETECTION OF OIL SPILLS BY SAR IMAGES - Dark Spot Detection and Feature Extraction

5) NAMES OF AUTHOR(S) IN FULL (surname first)

BREKKE Camillla

6) DISTRIBUTION STATEMENT

Approved for public release. Distribution unlimited. (Offentlig tilgjengelig)

7) INDEXING TERMS

IN ENGLISH:	IN NORWEGIAN:
a) Synthetic Aperture Radar	a) Syntetisk Aperture Radar
b) Oil spill	b) Oljesøl
c) Automatic algorithms	c) Automatiske algoritmer
d) Segmentation	d) Segmentering
e) Feature extraction	e) Egenskapsuttrekking

THESAURUS REFERENCE:

8) ABSTRACT

This report is written in the context of a PhD-study. The research is aiming at exploiting the potential of automatic detection of oil spills using new, advanced algorithms to demonstrate how well such a system will perform in terms of accuracy on a large set of SAR images. The approach to automatic oil spill detection has three main parts: dark spot detection, feature extraction and spot classification. This report covers some of the most recent contributions to the dark spot detector and the feature extractor.

9) DATE	AUTHORIZED BY This page only	POSITION
2005-04-15	Vidar S. Andersen	Director

UNCLASSIFIED

SECURITY CLASSIFICATION OF THIS PAGE
(when data entered)

CONTENTS

AUTOMATIC DETECTION OF OIL SPILLS BY SAR IMAGES - Dark Spot Detection and Feature Extraction

1 INTRODUCTION

Spaceborne Synthetic Aperture Radar (SAR) has proven to be the most efficient satellite sensor for oil spill monitoring of the worlds oceans. Oil spills correlate very well with the major shipping routes, and do often appear in connection to offshore installations. When taking into account how frequent illegal discharges from ships appear, controlled regular oil spills can be a much greater threat to the marine environment and the ecosystem than larger oil spill accidents like the Prestige tanker accident in 2002.

Oil spills appear as dark areas in the SAR images because the oil dampens the capillary waves on the sea surface. A part of the oil spill detection problem is to distinguish oil slicks from other natural phenomena (*look-alikes*) that dampen the short waves and create dark patches in a similar way. Oil slicks may include all oil related surface films caused by oil spills from oilrigs, leaking pipelines, passing vessels as well as bottom seepages, while look-alikes do include natural films/slicks, grease ice, threshold wind speed areas (wind speed < 3 m/s), wind sheltering by land, rain cells, shear zones, internal waves, etc. (6) (see figure 1.1 and figure 1.2). These ambiguities put a challenge on the selection of suitable features for oil spill detection.

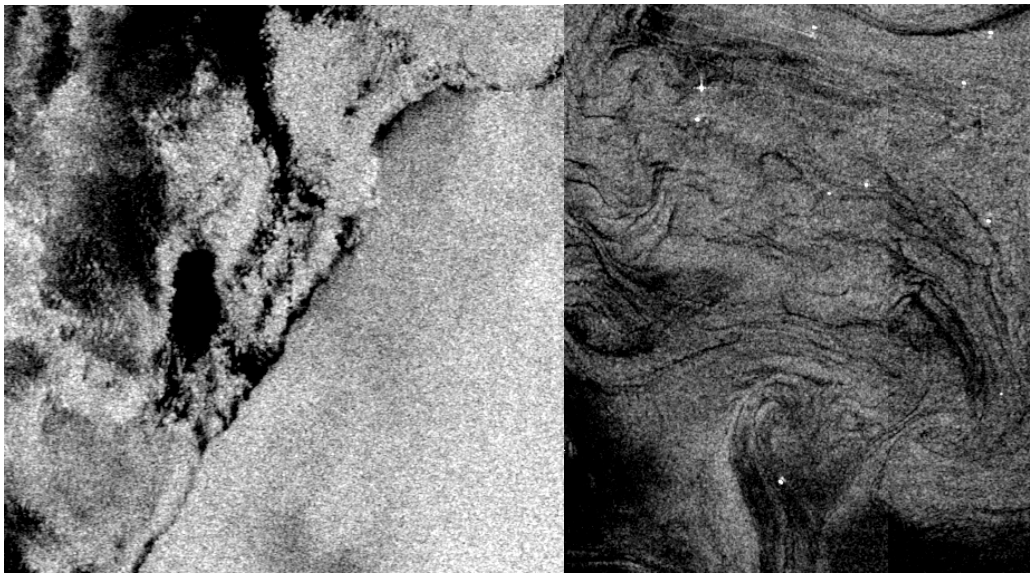

Figure 1.1 Examples of look-alikes that occur frequently in low wind areas. © ESA/KSAT 2003.

Figure 1.2 Section of an ENVISAT ASAR Wide Swath Mode (WSM) image (3 August 2003). Oil spill (indicated by arrow) surrounded by low wind look-alikes. The oil spill has been classified as oil by a German surveillance aircraft. © ESA/KSAT 2003.

Research in the field of automatic processing of SAR images, in order to detect illegal oil pollution, has been ongoing for more than a decade. Several papers, describing fully automatic or semi automatic systems, has been published, e.g. (1), (2) and (3). Little attention seems to have been given the feature extraction step, where parameters that can be used to discriminate oil spills from other phenomena appearing on the sea surface are extracted. An early study on feature extraction for oil spill detection based on ERS images is described by Solberg et al. (4), and an evaluation of the discrimination efficiency of typically used features can be found in Topouzelis et al. (5).

Segmentation of dark spots and feature extraction are a crucial part of algorithms for oil spill detection. If a slick is not detected during segmentation, it cannot be classified correctly. If the features have good discriminatory power, the classification problem will be easier and several classifiers can work. Keeping these issues in mind, results are hereby presented from a study aiming at identifying suitable features that lead to significant improvements in classification performance for ENVISAT ASAR WSM images. Improvements done to the dark spot detector are also described.

The content of this report has partly been published in (10), (8) and (14).

The report is organized in the following manner: section 2 covers a survey of related automatic techniques described in the literature for segmentation and feature extraction, our automatic oil spill detection algorithm is described in section 3, section 4 outlines the experiment design and presents the experimental results, and finally the conclusion can be found in section 5.

2 AUTOMATIC TECHNIQUES FOR DARK SPOT DETECTION AND FEATURE EXTRACTION

This section covers related algorithms and techniques described in the literature.

2.1 Segmentation techniques

As oil spills are characterized by low backscattering levels this suggest the use of thresholding for dark spot segmentation. An early attempt on segmentation of ERS-1 SAR images is described by Skøelv and Wahl (16). The algorithm simply looks for bimodal histograms in widows of size *N x N* pixels (*N* was sat to 25 pixels). This is reported as a good method for detection of oil spills provided that the spill is not too thin. A similar approach is briefly described in (17) and (18). This algorithm, which is developed for RADARSAT-1 SAR data, spatially averages the image before a user defined adaptive threshold is applied. As both these algorithms lack a classification step look-alikes will be detected as well.

The use of hysteresis thresholding was introduced by Canny (19) and is applied by Kanaa et al. (20) for detecting oil spills in ERS amplitude images. A search is done in the 8-neighbourhood directions followed by a merging step of the responses. Linear features are reported accentuated by this method.

An oil slick detection approach, based on the Laplace of Gaussian (LoG) and Difference of Gaussian (DoG) operators, is described in (21) and (24). The LoG operator is applied on the coarsest layer of a *2 x 2* pixel reduced pyramid with three layers. The concave areas of the grey level surface are selected. The DoG is used to locate those areas with more than half of the slick boundary pixels greater than $\mu + 1.75\sigma$ (as selected for ERS-1, where μ and σ are mean and standard deviation over all image pixels). To improve the result the finer layers of the pyramid are processed.

The use of wavelets in ocean feature detection (including oil spills) is described by Liu et al. (22) and Wu and Liu (23). In the general linear feature detection scheme the analysing wavelet is defined as the LoG. Regions with multiple histogram peaks are selected for the wavelet transform. The wavelet is applied as an edge detector as the contours of the zero crossing indicates the feature edges (see (19)).

As oil spills dampens the capillary waves, Mercier et al. (27) suggest a segmentation method based on detecting local variations of the wave spectra. First a multi-resolution analysis is achieved by a wavelet packet transform then a Hidden Markov Chain (HMC) model is applied to the wavelet coefficients. The technique is tested on an ERS Precision Image Mode (PRI) image.

QinetiQ's dark spot algorithm uses a Constant False Alarm Rate (CFAR) algorithm to locate dark regions. The dark spots are merged according to a clustering radius and a threshold, and the Hough transform is used specially to identify linear targets (7).

To allow dealing with mixed surface-cover classes and unsharp boundaries among regions, Barni et al. (25) propose an algorithm based on fuzzy clustering. A membership function $u_A(x)$ is assigned to each pixel x, which measures how much the pixel belongs to a set A. The Fuzzy C-means (FCM) algorithm is applied, and a pyramid structure is used in finding the membership values. Uncertain pixels are tested in the lower pyramid level. Neighbouring regions are identified, and a Sobel operator is used to enhance the main edges of the original filtered image. Regions, whose common border does not have a high enough percentage of large gradient points, are merged together. One difficulty with fuzzy clustering is to find the optimum number of clusters.

A method using mathematical morphology for oil spill segmentation is presented by Gasull et al. (26). Combinations of opening and closing[1] operations are used for oil spill filtering and thresholding. The algorithm aims at detecting spills from sailing tankers, and some features used are the elongatedness and dampening of the spill.

Even though a variety of methods are applied, the common goal is to detect all suspicious slicks and to preserve the slick shapes. The latter is of most importance for the success of discriminating oil spills from look-alikes in the following feature extraction and classification steps.

2.2 Slick features

From the thresholded dark spot image, feature extraction is used to extract parameters describing each slick. Table 2.1 summarizes the features used in three different algorithms: Frate et al. (1), Solberg et al. (3), and Fiscella et al. (2). Frate et al. apply a multiplayer perceptron (MLP) neural network classifier with two hidden layers, while Fiscella et al. compare a Mahalanobis classifier with a compound probability classifier in their study. The method of Solberg et al. is described in section 3.

[1] Opening: erosion followed by dilation. Closing: dilation followed by erosion (see (28) for an introduction to mathematical morphology).

Feature class	**#**	**Feature**	**1**	**2**	**3**
Geometry and shape	1	Slick area (*A*)	X	X	X
	2	Slick perimeter (*P*)	X		X
	3	*P/A*			X
	4	Slick complexity	X	X	
	5	Spreading (low for long thin slicks, high for circular shape)	X		
	6	Slick width		X	
	7	First invariant planar moment (9)		X	
	8	Dispersion of slick pixels from longitudal axis			X
Backscatter level and texture	9	Object/dark area standard deviation	X		X
	10	Background/outside dark area standard deviation	X		X
	11	Max contrast (between object and background)	X		
	12	Mean contrast (between object and background)	X		
	13	Max border gradient	X		
	14	Mean border gradient	X	X	
	15	Gradient standard deviation	X		
	16	Local area contrast ratio		X	
	17	Power-to-mean ratio of the slick		X	
	18	Homogeneity of surroundings		X	
	19	Average NRCS inside dark area			X
	20	Average NRCS in limited area outside dark area			X
	21	Gradient of the NRCS across the dark area perimeter			X
	22	Ratio #9 to #10			X
	23	Ratio #19 to #9			X
	24	Ratio #20 to #10			X
	25	Ratio #23 to #24			X
	26	Ratio #19 to #20			X
Contextual	27	Distance to a point source		X	
	28	Number of detected spots in the scene		X	
	29	Number of neighbouring spots		X	

Table 2.1 Features applied by various algorithms. 1: Frate et al. (1), 2: Solberg et al. (3), 3: Fiscella et al. (2). X *indicates that the parameter is used in the feature vector of the particular algorithm.*

In a feature vector that is input to the classifier, the individual features are typically covered by the following classes:

- *The geometry and shape of the segmented region.*
  Geometric and shape features are applied by all methods in table 2.1. To detect pollution from sailing tankers cleaning their tanks, an important feature is elongatedness that can be expressed as a ratio between the width and length of the slick

(26). Another possible feature useful in identifying these spots is the first invariant statistical moment of Hu (9).

- *Physical characteristics of the backscatter level of the spot and its surroundings.*
  Frate et al. (1) found that features containing most valuable information for classification by neural networks were features covering information on the gradient of the backscattering value when passing from background to spill (#13, #14 and #15). In addition, the background standard deviation (#10) was found important which is a parameter highly affected by the wind level and is generally high for natural sea slicks. Similarly in (2), features connected to the slick surroundings were found to be important due to the wind speed dependence of oil spill observations (these features could also be classified as contextual features).

- *Spot contextual features.*
  Examples are slick location relative to the shore and distance to ships and oilrigs. In the contextual analysis of the supervised discrimination algorithm described by Espedal (32) is a "hot-spot" pollution source database used. Improved classification results were found by Solberg and Volden (33) when the dark spots are classified in the context of their surroundings and weather information is incorporated. Espedal and Wahl (34) suggest using wind history information for slick classification and slick age estimation. Wind history can also be looked at as an indirect spot feature.

- *Texture.*
  In contradiction to the pixel intensity itself, texture provides information about the spatial correlation among neighbouring pixels. Assilzadeh and Mansor (35) describe an early warning system where texture features based on grey level co-occurrence matrices (GLCM)[2] are used. Homogeneity and Angular Second Moment were found effective in separation of oil spills from other objects. The Power-to-mean ratio of the slick and the surroundings are used by Solberg et al. (3) as a measure of homogeneity.

Even though the different methods in table 2.1 does not apply the exact same features are several of the features different measures of the same characteristic.

Fractal texture description can be used to describe natural surfaces (31). The use of fractal dimension[3] as a feature for classifying observed ocean radar signatures is suggested in (36). A box-counting algorithm (the method is described in (37)) is used to find the fractal dimension D. A difference in D of oil spills compared to other oceanic phenomena is reported found. In another paper on fractal dimension by Benelli and Garzelli (38) was a steady fractal dimension value of $D = 2.45$ found for the sea surface, while an average value of $D = 2.15$ was found for oil spills. A smaller D indicates less roughness.

[2] GLCM: approximates the grey level joint probability distribution (30).
[3] A surfaces fractal dimension corresponds closely to our intuitive notion of roughness (31).

Good features are important, but the lack of good guidelines on how to acquire them has been pointed out by Kubat et al. (29).

3 THE AUTOMATIC OIL SPILL DETECTION ALGORITHM

The framework of this study is a fully automatic advanced oil spill detection algorithm developed in cooperation between Norwegian Computing Center (NR) and University of Oslo. It was originally intended to process ERS-1/-2 SAR images, but has now been extended to work for RADARSAT-1 SAR and ENVISAT ASAR images. The algorithm includes sensor specific modules for dark spot detection, spot feature extraction and a classifier that discriminates between oil spills and look-alikes (see figure 3.1).

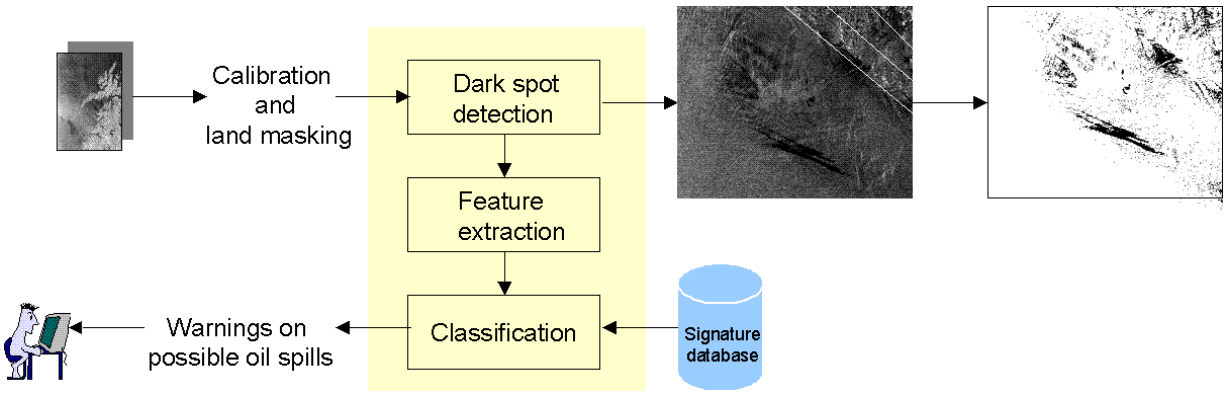

Figure 3.1 The automatic oil spill detection system and its context. Arrows indicates data flow.

Pre-processing, consisting of converting a land mask to the image grid (to avoid re-sampling the speckle pattern) and a normalization of the backscatter with respect to incidence angles, is performed ahead of the segmentation step for ENVISAT ASAR images.

3.1 Dark spot detection

The dark spot detector applies an adaptive threshold where the threshold is set k dB below the local mean backscatter level in a large window. The details can be found in (10) and (3). The goal of this step is to segment out all possible oil spill candidates. A high number of look-alikes will also be segmented out, but these will hopefully be classified as look-alikes during the classification step. The thresholding is done in a two level pyramid after applying a simple speckle filter with a small window. k is determined based on the wind level. If no wind information is available, we use the power-to-mean (PMR) ratio of the local surroundings as an indication of the number of look-alikes in the scene. The number of observed look-alikes

will vary according to local wind conditions. See figure 3.2 for an example on how the dark spot algorithm works.

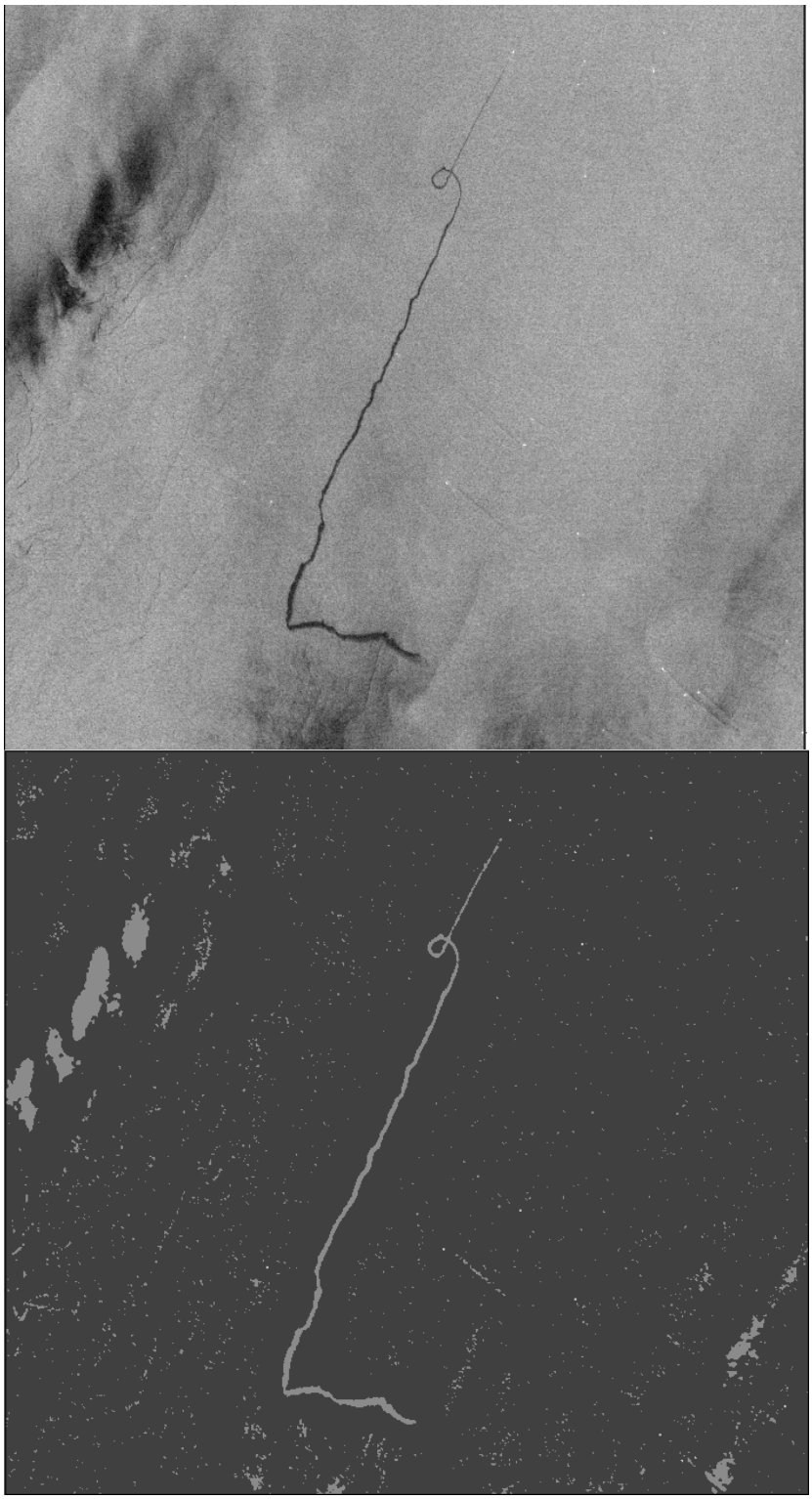

Figure 3.2 *Top: section of an ENVISAT ASAR WSM scene (16 September 2003) © ESA/KSAT 2003. A long oil spill with a loop is clearly visible. A likely source can be seen at the upper end of the spill. Bottom: segmentation result. The oil spill, in addition to several other dark phenomena, has been separated from the background.*

3.1.1 Detection of thin, linear slicks

The procedure above works very well in general, but in some cases it does not work for thin, linear slicks. A new approach has been developed for ENVISAT ASAR WSM images for detecting these cases. The image is thresholded with the approach described above, but by fixing *k* at a small dB value. This gives an image with too many object pixels, and it is only used to locate fragments that can be part of a linear oil spill. Hu's 1st invariant planar moment (9) is a good indicator of elongatedness, and fragments with a moment value > 0.5 are selected for further processing. The ratio between the width and the length of the slick is used to eliminate broad fragments. For every fragment an object-oriented bounding box B_1 is found. B_1 is extended in both directions of the fragments orientation during the search for additional object pixels. A sigma filter is used for slight noise filtering of the ASAR image before applying the following equation as a threshold inside B_1: $T = \mu_{B_2} - l$, where μ_{B_2} is the mean value found inside an object-oriented bounding box B_2 with increased width and l is a small selected dB value. If the backscatter value of a pixel is < T it will only be accepted if it selves or one of its 8-neighbour pixels represents an edge pixel (using Sobel convolution kernels). The segmented slick is added to the original segmented image. Figure 3.3 shows that fragments are merged and that the shape of the thin, linear slick is preserved by this approach.

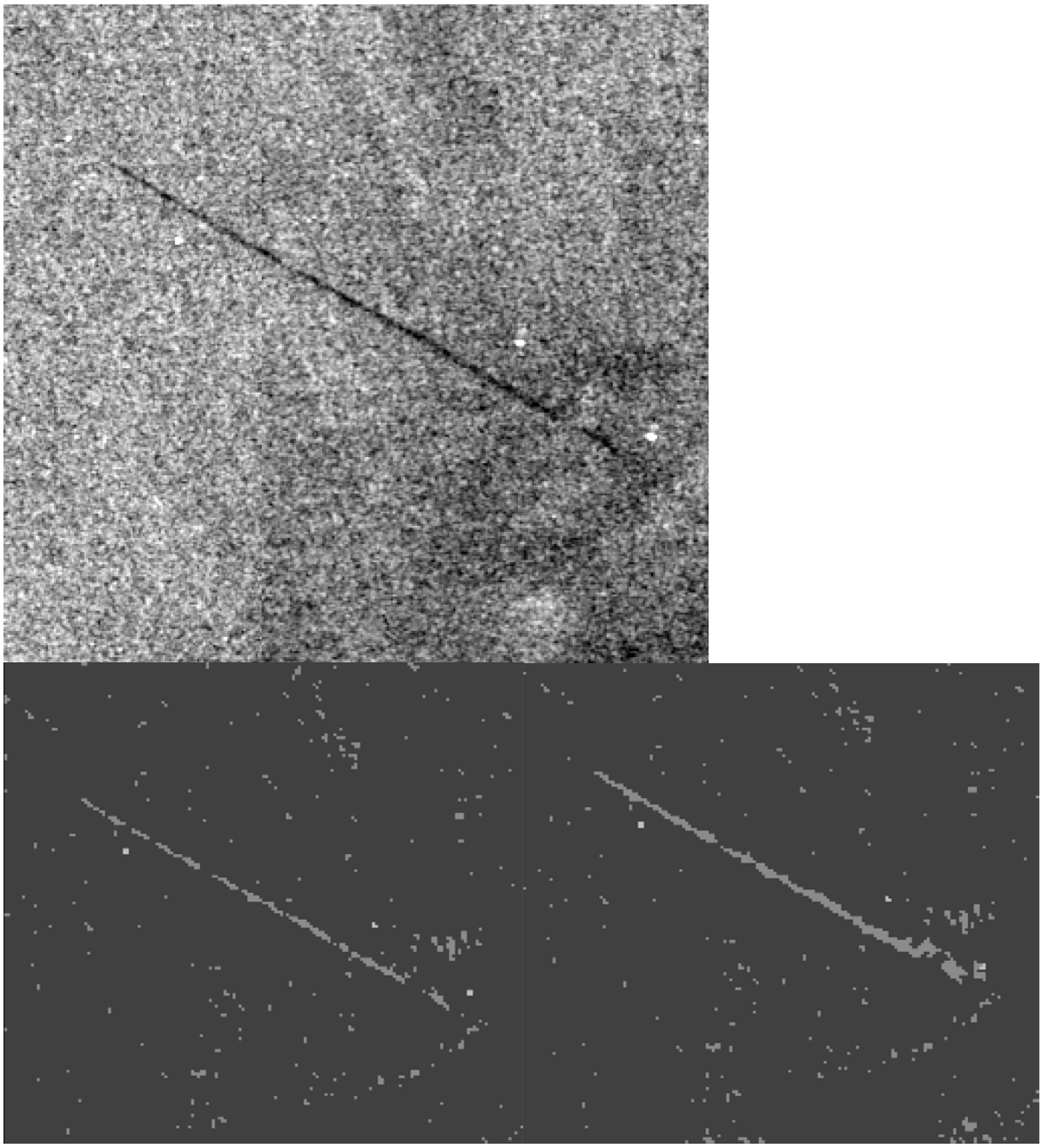

Figure 3.3 Top: section of an ENVISAT ASAR WSM image (19 September 2003). Bottom, left to right: original segmentation result and the improved result from the object-oriented bounding box approach.

Figure 3.4 shows another oil spill affected by this approach.

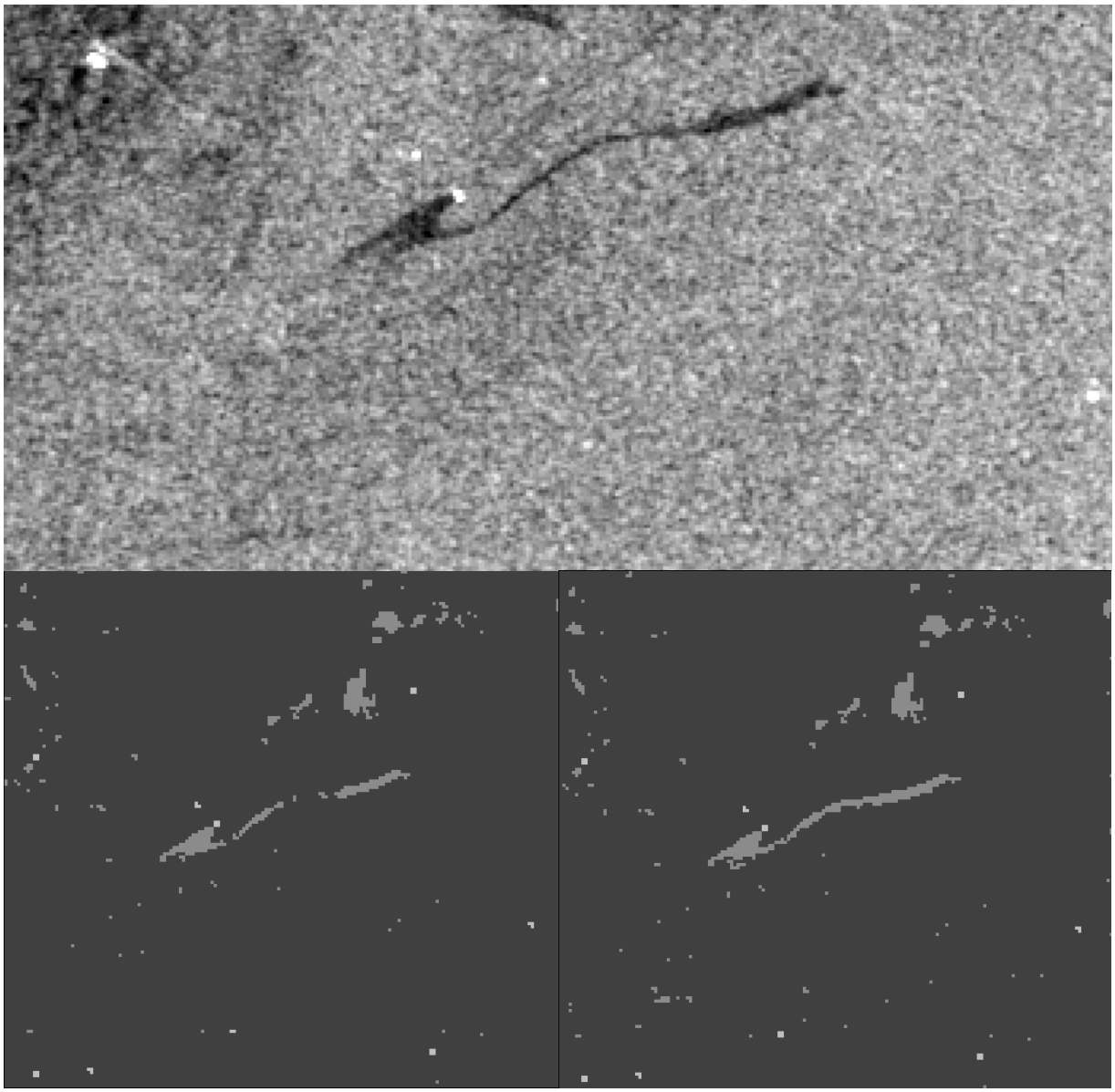

Figure 3.4 Top: section of an ENVISAT ASAR WSM image (17 August 2003). Bottom, left to right: original segmentation result and the improved result from the object-oriented bounding box approach.

3.2 Slick feature extraction

After the segmentation process, a set of features are computed and extracted from every region above a certain minimum size.

3.2.1 Existing set of features

A basic set of features was described in (3). The features are a mix of standard region descriptors and features tailored to oil spill detection (see table 3.1). Not all of these features

were found to be robust and yield the best description of the type of information it was meant to extract. A goal of this work is to find new features and compare their performance to the existing.

Feature #	**Feature**	**Description**
1	WIND	The wind level in the scene.
2	MOM (Moment)	1st planar moment of the region.
3	COMPL (Slick complexity)	Defined as $C = P^2 / A$, where P is the perimeter and A is the area of the region.
4	PMR (Power-to-mean ratio)	Homogeneity of the regions surroundings, defined as the ratio of standard deviation, σ_b, and the mean, μ_b, of near-by background pixels surrounding the region.
5	LCONT (Local contrast)	Local area contrast, defined as $\mu_b - \mu_r$, where μ_b is the background pixel mean and μ_r is the region pixel mean.
6	THICK (Thickness)	Thickness of the region, defined as the ratio between the area of the region and the diameter of the region skeleton.
7	NOFSN (Number of small neighbours)	The number of small neighbouring regions.
8	BGRAD (Border gradient)	The mean of the magnitude of the region border gradient. Sobel is used to compute the gradients.
9	SMC (Smoothness contrast)	Defined as the ratio between the ratio of the number of region pixels and the sum of the region gradient values, and the ratio of the number of background pixels and the sum of the background gradient values.
10	AREA	The number of pixels in the region.
11	DIST (Distance)	The distance from the region to closest bright spot (ship).
12	NLN (Number of large neighbours)	The number of large neighbouring regions.
13	NREG (Number of regions)	The total number of detected regions in the scene.

Table 3.1 Basic feature vector components. The features are based on geometrical characteristics, texture, the backscatter level, and contextual information.

3.2.2 New features

The basic feature set has been extended with the features described in the following.

3.2.2.1 Slick border gradient

The Sobel operator is an edge detector that has been suggested used for oil spill border gradient estimation, see e.g. (11) and (3). Originally the mean value of the magnitude was applied in the BGRAD feature in our system (see table 3.1). It works generally well, but it seems to give inaccurate results for thin linear regions. The main problem is that the edge response does not match the real borders of the region. The top row to of figure 3.6 illustrates the response of the Sobel operator on the oil spill in figure 3.5. As we can see, the largest gradient magnitude appears outside the true region border.

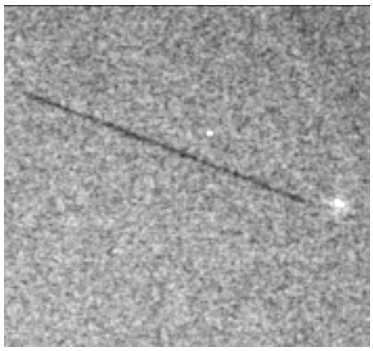

Figure 3.5 Section of an ENVISAT ASAR WSM image (24th of July 2003). A possibly thin linear oil spill with a likely source is visible.

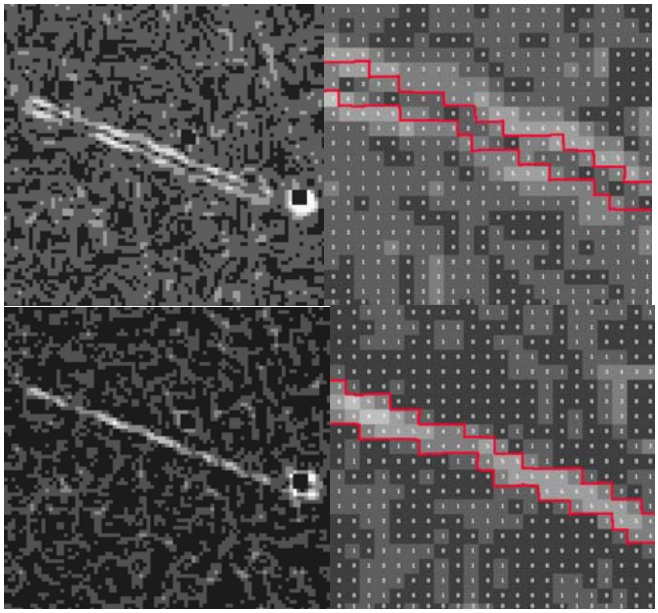

Figure 3.6 *Top row: the Sobel operator yields the largest border gradient magnitude response outside the region border. The gradient is misplaced according to the real border of the region (indicated by the red lines). Bottom row: response from improved border gradient estimation.*

The following 4 additional convolution masks are suggested for gradient estimation of thin oil spill regions:

$$\begin{bmatrix} 0 & 0 & 0 & 0 & 0 \\ 0 & 0 & 0 & 0 & 0 \\ 1 & 1 & -4 & 1 & 1 \\ 0 & 0 & 0 & 0 & 0 \\ 0 & 0 & 0 & 0 & 0 \end{bmatrix}, \begin{bmatrix} 0 & 0 & 1 & 0 & 0 \\ 0 & 0 & 1 & 0 & 0 \\ 0 & 0 & -4 & 0 & 0 \\ 0 & 0 & 1 & 0 & 0 \\ 0 & 0 & 1 & 0 & 0 \end{bmatrix}, \begin{bmatrix} 0 & 0 & 0 & 0 & 1 \\ 0 & 0 & 0 & 1 & 0 \\ 0 & 0 & -4 & 0 & 0 \\ 0 & 1 & 0 & 0 & 0 \\ 1 & 0 & 0 & 0 & 0 \end{bmatrix} \text{ and } \begin{bmatrix} 1 & 0 & 0 & 0 & 0 \\ 0 & 1 & 0 & 0 & 0 \\ 0 & 0 & -4 & 0 & 0 \\ 0 & 0 & 0 & 1 & 0 \\ 0 & 0 & 0 & 0 & 1 \end{bmatrix}$$

The magnitude of the pixel gradient is found by $\nabla(p) = \max\{\nabla(p)_i : i = 1 \text{ to } 4\}$, where p = current pixel, i = mask. The bottom row of figure 3.6 illustrates the response to these masks. If the Sobel operator gives stronger magnitude response to any of the border pixels that value is kept, otherwise the response from the additional masks is used. The mean of this border gradient detector gives us an indication of the contrast to the surrounding background, and it is used in the improved feature BGRAD_NEW to replace the BGRAD feature in table 3.1.

3.2.2.2 Texture

Texture refers to the properties that represent the surface or structure of an object, but there is no precise mathematical definition of texture due to its wide variability. In table 3.1 there is no feature representing the texture of the slick it self. Solberg et al. (3) have earlier suggested the PMR of the slick, defined as σ_r / μ_r where σ_r is the standard deviation and μ_r is the mean value of the slick. Frate et al. (1) have simply used the standard deviation of the slick as a texture measure. However, the standard deviation of the intensity values of the pixels belonging to a slick is highly correlated with the area/size of the region. This is due to the inherent nature of speckle statistics. Speckle is a large problem in SAR images since even a homogeneous area has a statistical distribution with large standard deviation. As the region grows larger the variance in intensity values will increase as well. A better choice would be to look at the ratio σ_r^2 / A, where σ_r is the standard deviation and A is the area of the slick. After normalization by area, the measured feature values of larger oil spills are comparable to smaller samples.

3.2.2.3 Geometrical complexity

Features, based on the ratio between the perimeter and the area, aiming at describing the shape complexity of regions have been used in several algorithms described in the literature (2), (3), (1), and (5). In (3) the complexity feature is implemented as $C = P^2 / A$ (see table 3.1) while in (1) it is implemented as $C = P / 2\sqrt{\pi A}$, where P is the perimeter and A is the area of the region[4]. Generally, this feature is expected to get a small numerical value for regions with simple geometry, while a larger value for more complex regions. In contradiction to common intuition, the thin linear oil spill in the bottom of figure 3.7 gets a larger complexity value than

[4] This quantity is referred to as *compactness* in (12). It measures the ratio between the area of the shape and the circle that can be traced with the same perimeter: $C = 4\pi A / P^2$.

both the others when using the formula in table 3.1. Frate et al.'s (1) formula gives very similar but differently scaled results.

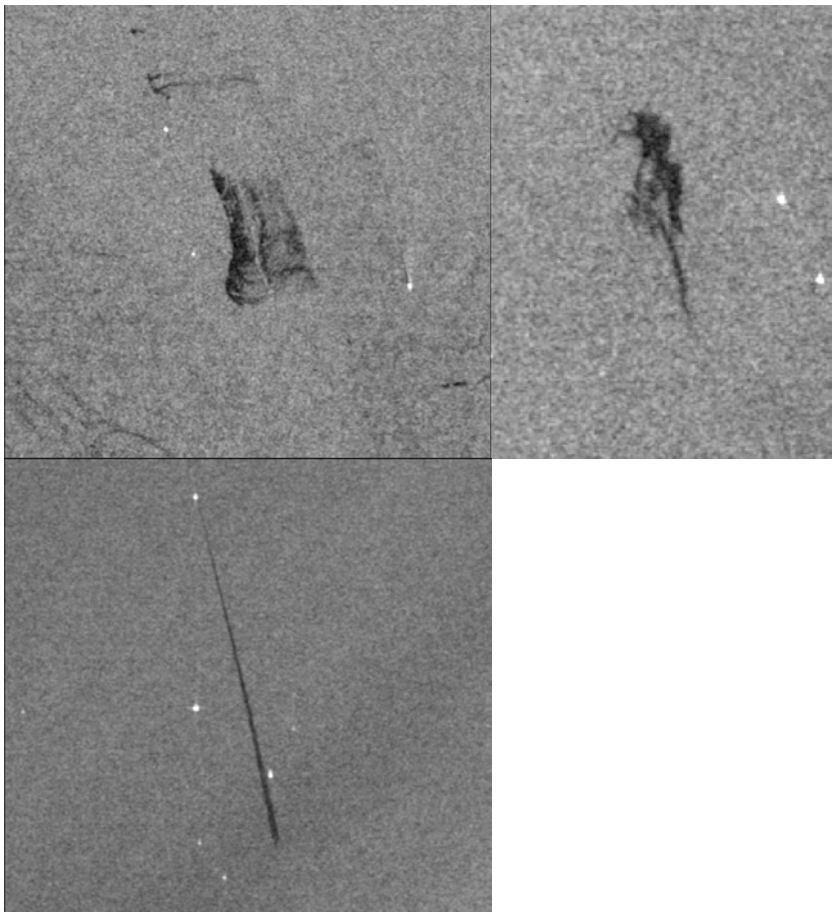

Figure 3.7 Section of ENVISAT ASAR WSM images. Top left: 8th of March 2003. Top right: 7th of August 2003. Slicks with wide, complex, irregular shapes. Bottom: 12th of February 2003. Thin, linear oil spill with a regular shape.

This indicates that the ratio between perimeter and area is not a good complexity measure as it is not possible to separate complex shaped slicks from linear slicks. This weakness is also pointed out by Nixon and Aguado (12), and Topouzelis et al. (5) found that the feature gave little contribution to oil spill detection.

To resolve this ambiguity we could introduce additional shape measures, or replace this measure with a more robust one. A possibility is to look at the number of branching points[5] in the skeleton of each region (see figure 3.8). Because we only look at the number of branching points, the information level is decreased so much that again it is often not possible to distinguish simple regions from more complex ones (e.g. a straight line would get the same feature value as an “S” shaped region). It is clear that it is important to preserve more shape information in features expressing geometrical complexity.

[5] We define *the number of branching points* as a point with three lines or more connected to it.

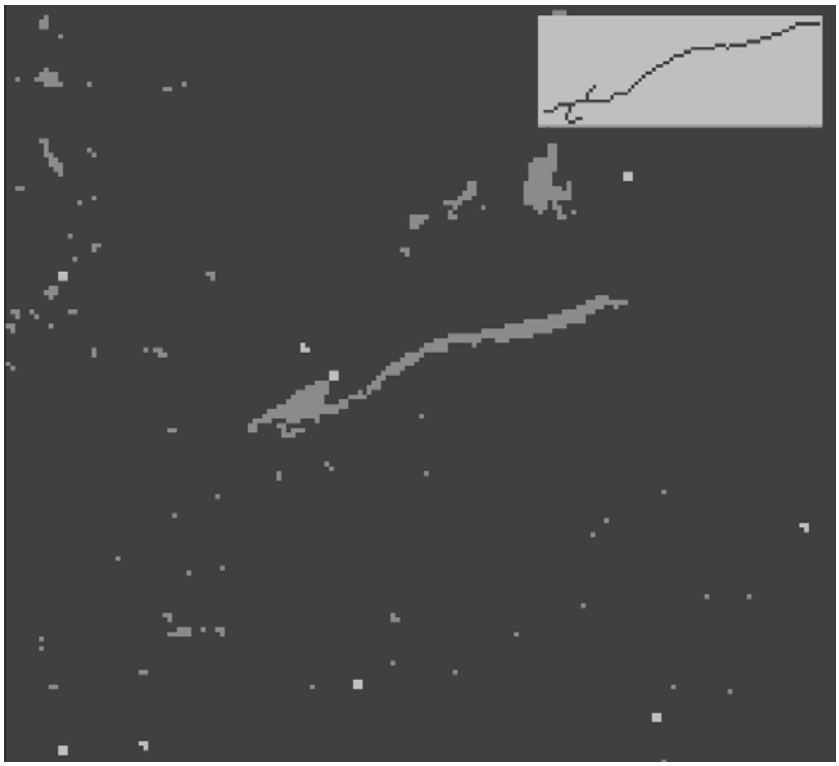

Figure 3.8 Segmentation result of the oil spill in figure 3.4 and its skeleton (upper right corner).

Contour or snake models are commonly applied to ultrasound image segmentation. Lobregt and Viergever (13) define local curvature $\vec{c}_i$ as the difference between the directions of two edge segments that join at a vertex: $\vec{c}_i = \hat{d}_i - \hat{d}_{i-1}$ (see figure 3.9). The local curvature has length and direction. This provides a measure of the angle between two joining edge segments. The length of the curvature vector depends only on this angle and is not influenced by the lengths of the two edge segments.

In our implementation of the curvature feature, we have traced the boundary of every region and inserted vertexes with a three-pixel spacing. The angle between two edge segments is calculated as described above, and the final CURVATURE feature is the sum of all local curvature measures along the boundary. More complex regions get a higher curvature measure.

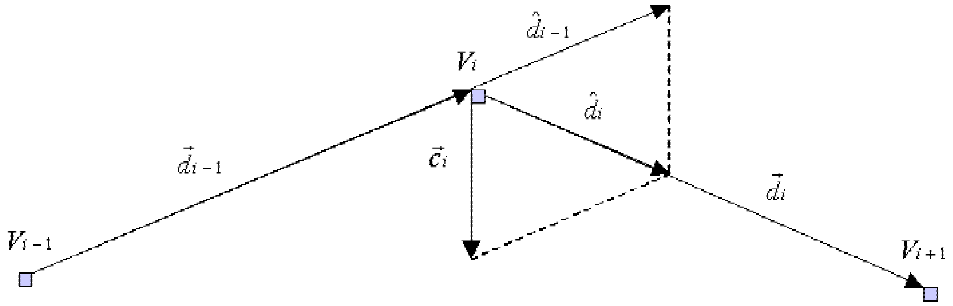

Figure 3.9 Local curvature $\vec{c}_i$. $\hat{d}_{i-1}$ and $\hat{d}_i$ are the directions (unit vectors) of the edge segments $\vec{d}_{i-1}$ and $\vec{d}_i$ meeting at vertex V_i.

3.3 Statistical classification

After a set of *M* dark spots has been detected, we want to classify them as either oil spills or look-alikes. For this purpose, a classification algorithm has been developed, combining a statistical model for oil spills of different shapes and seen under different wind conditions, a prior model for the probability of observing oil and look-alikes, and a rule-based approach which take care of certain expert knowledge related to oil spill detection (3). Only the features COMPL, PMR, LCONT, THICK, NOFSN, BGRAD, and SMC from table 3.1 are used to compute the probability densities. The WIND and MOM features are used to group the samples first in two different subclasses based on wind, and then five different subclasses for each wind level according to their value of the shape descriptor. The rest of the features are included in rule-based corrections of the class-conditional densities. The classifier is trained (that is, the means and the covariance matrices in the Gaussian densities are estimated) on a large set of labelled samples. Diagonal covariance matrices are used because the number of oil spills in each sub class is small.

4 PERFORMANCE TESTING

ENVISAT's ASAR WSM covers a much wider swath than its predecessors ERS-1 and -2, but the resolution is significantly lower. Generally, for efficient oil spill monitoring larger swath widths should be chosen on the expense of somewhat lower resolution. C-band single-polarized VV SAR has so far proven to be the most efficient configuration for oil spill detection (39), but no significant difference in practical performance between the detection capabilities of the HH-polarized RADARSAT-1 SAR versus ENVISAT ASAR has yet been reported for operational use, however the experience might still be limited. Because of ENVISAT's good oceanography and oil spill detection properties, we have chosen its WSM mode for our experimental design.

4.1 Experimental design

Our results are based on a large set of 83 ENVISAT ASAR WSM images. We have benchmark results and aircraft verifications collected by the European Commission (EC) project Oceanides for 27 of the scenes. This is done in collaboration with Kongsberg Satellite Services (KSAT), QinetiQ, NR, German pollution control authorities (MLZ) and Finnish pollution control authorities (SYKE) (see (7)). For performance testing, the set of SAR scenes is split into two parts. 56 of the SAR scenes are used for training and adjusting the model parameters, and the 27 benchmark scenes are used as a validation/test set to estimate the generalization error. The training set is collected from the German and Finnish Baltic Sea, the North Sea and some along the Norwegian coastline during March to December 2003 and

January to April 2004. The benchmark set is collected mainly from the German and Finnish Baltic Sea and the German North Sea between July and December 2003.

4.2 Intermediate results – improved dark spot detection

After improving the dark spot detection of thin, linear slicks (as described in section 3.1.1), the *leave-one-out*[6] method was applied to the training set to get a large range of fragmented, linear cases to test the algorithm on. A total of 16 linear oil spills were tested, and the classification results are presented in table 4.1.

Method	**Correctly classified thin, linear oil spills**
Original dark spot detector	75%
Improved dark spot detector	88%

Table 4.1 Classification by the leave-one-out method of 16 linear oil spills from the training set.

The feature vector from table 3.1 and all rule-based corrections of the class-conditional densities, see (3), were applied in the classifier. Figure 4.1 presents one of the cases that were missed earlier, but classified correctly as oil spill after introducing the improvements from section 3.1.1 to the dark spot detector. The improvements were also included in the algorithm when we generated all benchmark results presented in the next section.

[6] See e.g. (15) for a description of the method.

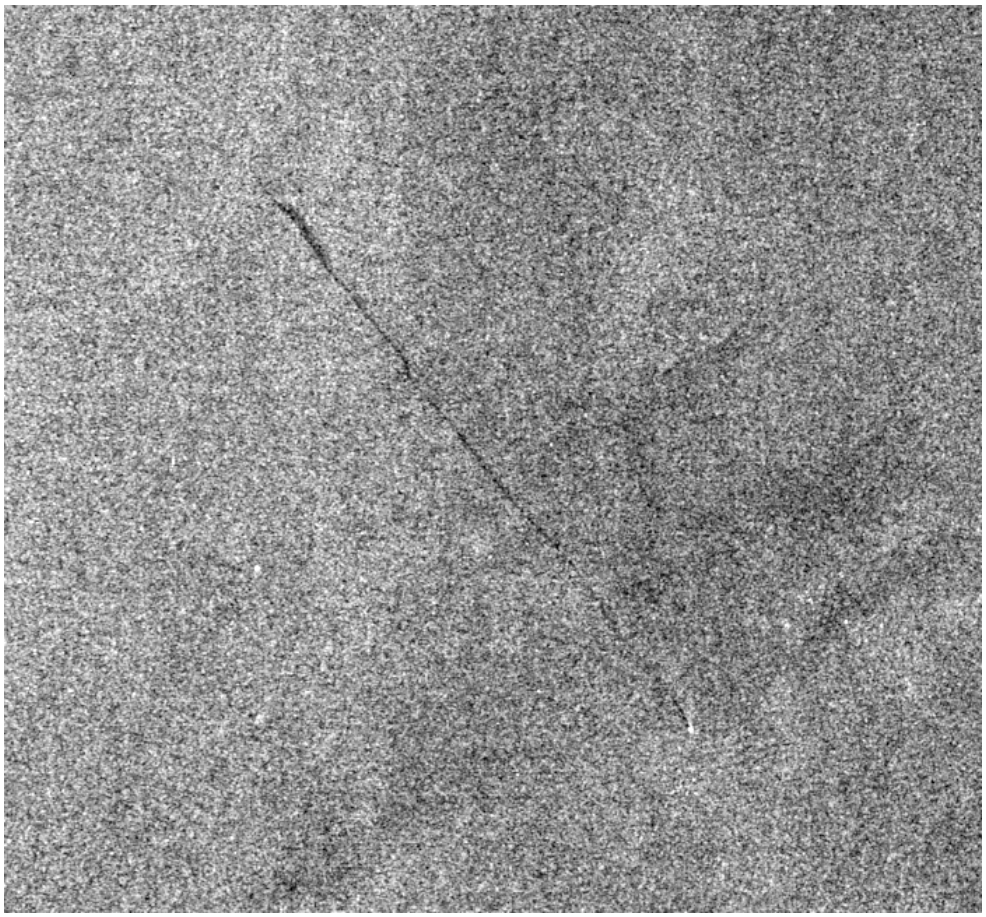

Figure 4.1 Section of an ENVISAT ASAR WSM image (25 August 2003) © ESA/KSAT 2003. Example of a thin, linear slick that was correctly detected as oil spill after the improvements to the dark spot detector was introduced.

4.3 Classification results

Table 4.1 presents the results from classifying the complete benchmark set of 27 scenes by applying feature #3 - #9 in table 3.1.

Basic feature set	Correctly classified oil spills	Correctly classified look-alikes
#3 - #9	89 %	90 %

Table 4.1 Classification results based on the basic set of features.

A doubt category was used to mark slicks we were uncertain about. These cases are left out of the classification results. The classification was done without the rule-based corrections of the class-conditional densities described in Solberg et al. (3). The rule-based corrections are based on the observed values of the basic set of features on the training set. When replacing some of the features, the rules have to be modified. This is not done in the current analysis, but will be done in the near future. Thus, the rule-based corrections are left out of all performance results

hereby presented. The results in table 4.1 can for this reason be used as a reference for table 4.3 and 4.4.

Table 4.2 gives a definition of the new set of features.

Feature #	Feature	Description
14	BGRAD_NEW	The mean border gradient. A combination of Sobel and the four additional masks described in section 3.2.2.1 is used as a gradient detector.
15	VAR_AREA_SLICK	Defined as the ratio σ_r^2 / A, where σ_r is the standard deviation and A is the area of the slick.
16	CURVATURE	Defined as the sum of all local curvature measures (changes of slope) along the boundary.

Table 4.2 Extended set of features.

Tabell 4.3 presents intermediate results after introducing one at the time of the new features from table 4.2.

Feature set	Correctly classified oil spills	Correctly classified look-alikes
#3, #4, #5, #6, #7, #14, #9	95%	88%
#3, #4, #5, #6, #7, #8, #9, #15	92%	89%
#16, #4, #5, #6, #7, #8, #9	92%	89%

Tabell 4.3 Intermediate results.

By introducing each of the new features, the number of correctly classified oil spills is increased, while the number of look-alikes correctly classified is decreased compared to table 4.1.

The results from a forward selection of the features #3 - #13 in table 3.1 in addition to the new features in table 4.2 (#14 - #16) is plotted in figure 4.2.

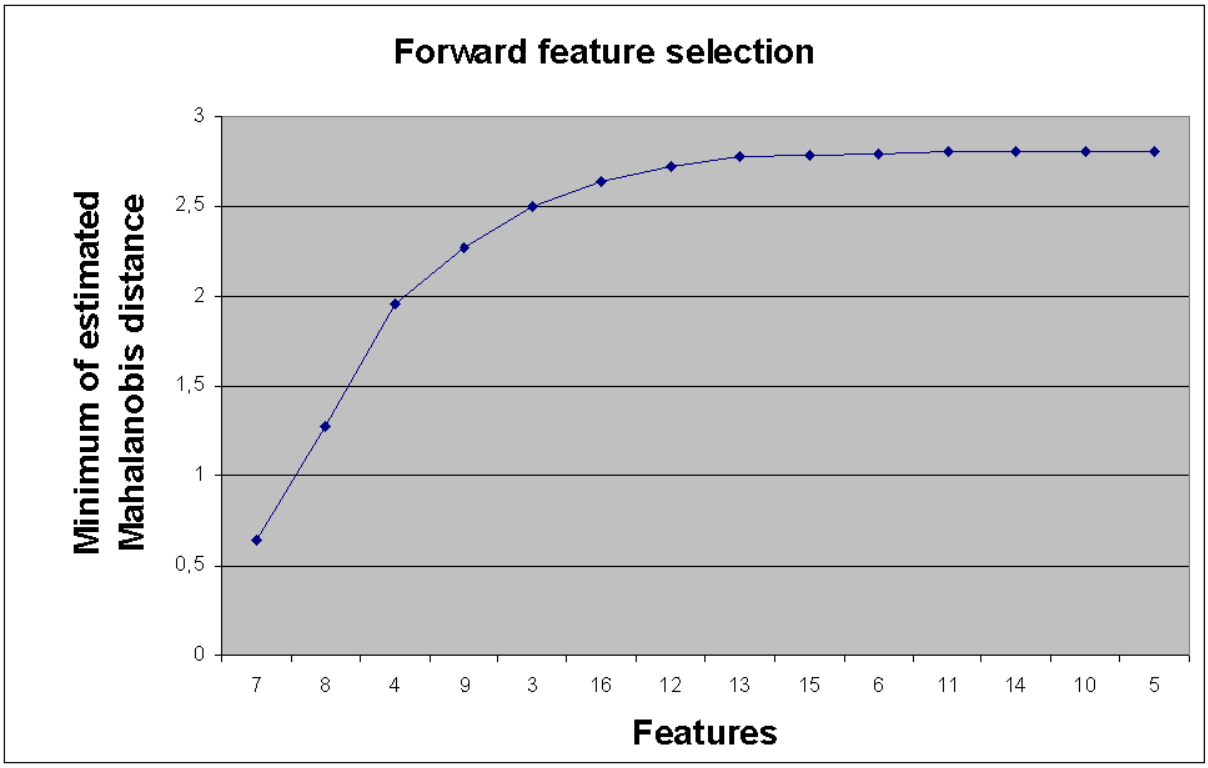

Figure 4.2 *Forward feature selection of 14 features according to the minimum estimated Mahalanobis distance. 3: COMPL, 4: PMR, 5: LCONT, 6: THICK, 7: NOF_SMALL_NEIGHB, 8: BGRAD, 9: SMOOTH_CONTR, 10: AREA, 11: DIST, 12: NOF_LARGE_NEIGHB, 13: NOF_REGIONS, 14: BGRAD_NEW, 15: VAR_AREA_SLICK and 16: CURVATURE.*

As the figure illustrates, adding more and more features gives little added value to the performance results. More research on which combination of features is the most optimal for oil spill detection is needed.

Table 4.4 presents the final classification results after substituting the COMPL feature in table 3.1 with CURVATURE, BGRAD with the improved border gradient detector BGRAD_NEW, and adding the VAR_AREA_SLICK as an additional feature to the feature vector.

New feature set	**Correctly classified oil spills**	**Correctly classified look-alikes**
(#16, #4, #5, #6, #7, #14, #9 and #15)	97 %	90 %

Table 4.4 *Classification results based on the new feature vector.*

5 CONCLUSION

In this report we have presented experimental results from an evaluation of features for oil spill detection based on SAR images. We have studied properties of the border gradient and texture

measures of the slicks. These are features based on the backscatter level characteristics of the slicks and their surroundings. In addition, we have compared several features measuring geometrical complexity of the slick. The use of curvature, as adopted from the well-known concepts of contour models (snakes), is suggested as a more robust complexity feature than those commonly applied in the oil spill remote sensing literature.

The features have been evaluated on a large set of 83 ENVISAT ASAR WSM images, achieving an improvement from 89% to 97% in the number of suspected slicks classified correctly as oil spills. Further research should focus on increasing the number of 90% correctly classified look-alikes, i.e. decreasing the false alarm rate. The rule-based corrections left out in this experiment need be to modified according to the new set of features, because the rule-based corrections are important in reducing the number of false alarms.

The features extracted vary between methods, and our future work will also include a comparison between our final selection of features and other feature combinations suggested in the literature.

6 ACKNOWLEDGMENTS

This work is performed as part of a PhD study funded by Norwegian Research Council and Norwegian Defence Research Establishment. The author would like to thank the Oceanides project for the ENVISAT ASAR scenes used in this work. The author would also like to thank Associate professor Anne H. S. Solberg at University of Oslo, Department of Informatics for her guidance and support.

References

(1) F. D. Frate, A. Petrocchi, J. Lichtenegger, and G. Calabresi (2000): Neural Network for Oil Spill Detection Using ERS-SAR Data, *IEEE Transactions on Geoscience and Remote Sensing,* **38**, 5, 2282-2287.

(2) B. Fiscella, A. Giancaspro, F. Nirchio, P. Pavese, P. Trivero (2000): Oil spill detection using marine SAR images, *Int. J. Remote Sensing,* **21**, 18, 3561-3566.

(3) A. H. S. Solberg, G. Storvik, R. Solberg, and E. Volden (1999): Automatic Detection of Oil Spills in ERS SAR Images, *IEEE Transactions on Geoscience and Remote Sensing,* **37**, 4, 1916-1924.

(4) A. H. S. Solberg and R. Solberg (1996): A Large-Scale Evaluation of Features for Automatic Detection of Oil Spills in ERS SAR images, Conference proceedings, IGARSS'96, 3, 1484-1486.

(5) K. Topouzelis, V. Karathanassi, P. Pavlakis, and D. Rokos (2003): Oil Spill Detection: SAR Multi-scale Segmentation & Object Features Evaluation, Remote sensing of the ocean and sea ice, 23-27 September, Crete, Greece, Conference proceedings, SPIE, 4880, 77-87.

(6) H. A. Espedal (1998): Detection of oil spill and natural film in the marine environment by spaceborne Synthetic Aperture Radar. PhD thesis, Department of Physics, University of Bergen and Nansen Environment and Remote Sensing Center, Norway.

(7) M. Indregard, A. Solberg, and P. Clayton (2004): D2-report on benchmarking oil spill recognition approaches and best practice. Technical report, Oceanides project, European Commission, Archive No. 04-10225-A-Doc, Contract No: EVK2-CT-2003-00177.

(8) C. Brekke and A. H. S. Solberg (2005): Oil spill detection by satellite remote sensing, *Remote Sensing of Environment,* **95**, 1, 1-13.

(9) M.-K. Hu (1962): Visual Pattern Recognition by Moment Invariants, *IEEE Trans. on Inf. Theory,* **8**, 179-187.

(10) A. S. Solberg, C. Brekke, R. Solberg, and P. O. Husøy (2004): Algorithms for oil spill detection in Radarsat and ENVISAT SAR images, Conference proceedings, IGARSS'04, Anchorage, Alaska, 20-24 September, 7, 4909-4912.

(11) F. Girard-Ardhuin, G. Mercier, and R. Garello (2003): Oil slick detection by SAR imagery: potential and limitation, Conference proceedings, OCEANS, 1, 164-169.

(12) M. Nixon and A. Aguado (2002): Feature Extraction & Image Processing, Newnes.

(13) S. Lobregt and M. A. Viergever (1995): A discrete dynamic contour model, *IEEE Transactions on Medical Imaging,* **14**, 1, 12-24.

(14) C. Brekke and A. H. S. Solberg (2005): Feature Extraction for Oil Spill Detection Based on SAR Images, Accepted at 14th Scandinavian Conference on Image Analysis, Joensuu, Finland, June 19-22, 2005. To be published in: Lecture Notes in Computer Science, ISSN 0302-9743 by Springer.

(15) R. O. Duda, P. E. Hart and D. G. Stork (2001): Pattern Classification, John Wiley & Sons.

(16) Å. Skøelv and T. Wahl (1993): Oil spill detection using satellite based SAR, Phase 1B completion report, Norwegian Defence Research Establishment

(17) P. W. Vachon, S. J. Thomas, J. A. Cranton, C. Bjerkelund, F. W. Dobson and R. B. Olsen (1998): Monitoring the costal zone with the RADARSAT satellite, Conference proceedings, Oceanology International 98, UK, March 10-13.

(18) M. J. Manore, P.W Vachon, C. Bjerkelund, H. R. Edel and B. Ramsay (1998): Operational use of RADARSAT SAR in the costal zone: The Canadian experiment, Conference proceedings, 27th International Symposium on Remote Sensing of the Environment, Tromsø, Norway, June 8-12, 115-118.

(19) J. Canny (1986): A computational approach to edge detection. , *IEEE Transactions on Pattern Analysis and Machine Intelligence*, **PAMI 8**, 6, 679-698.

(20) T. F. N. Kanaa, E. Tonye, G. Mercier, V. Onana, J. Ngono, P. Frison et al. (2003): Detection of oil slick signatures in SAR images by fusion of hysteresis thresholding responses, Conference proceedings, IGARSS'03, 4, 2750-2752.

(21) L. Y. Change, K. Chen, C. Chen, and A. Chen (1996): A multiplayer-multiresolution approach to detection of oil slicks using ERS SAR image, Conference proceedings, ACRS 1996 - 17th Asian Conference on Remote Sensing, Sri Lanka.

(22) A. K. Liu, C. Y. Peng and S. Y.-S. Chang (1997): Wavelet analysis of satellite images for costal watch, *IEEE Journal of Oceanic Engineering,* **22**, 1, 9-17.

(23) S. Y. Wu and A. K. Liu (2003): Towards an automated ocean feature detection, extraction and classification scheme for SAR imagery, *International Journal of Remote Sensing,* **24**, 5, 935-951.

(24) C. F. Chen, K. S. Chen, L. Y. Chang and A. J. Chen (1997): The use of satellite imagery for monitoring coastal environment in Taiwan, Conference proceedings, IGARSS'97, 3, 1424-1426.

(25) M. Barni, M. Betti and A. Mecocci (1995): A fuzzy approach to oil spill detection on SAR images, Conference proceedings, IGARSS'95, 1, 157-159.

(26) A. Gasull, X. Fabregas, J. Jimenez, F. Marques, V. Moreno and M. Herrero (2002): Oil spills detection in SAR images using mathematical morphology, Conference proceedings, EUSIPCO'2002, Toulouse, France, September, 1, 25-28.

(27) G. Mercier, S. Derrode, W. Pieczynski, J.-M. L. Caillec and R. Garello (2003): Multiscale oil slick segmentation with Markov Chain Model, Conference proceedings, IGARSS'03, 6, 3501-3503.

(28) M. Sonka, V. Hlavac and R. Boyle (1999): Image processing, analysis, and Machine vision, Brooks/Cole publishing.

(29) M. Kubat, R. C. Holte and S. Matwin (1998): Machine learning for the detection of oil spills in satellite radar images, *Machine Learning*, **30**, 195-215.

(30) R. M. Haralick (1979): Statistical and structural approaches to texture, Proceedings of the IEEE, 67, 786-804.

(31) A. P. Pentland (1984): Fractal-based description of natural scenes, *IEEE Transactions on Pattern Analysis and Machine Intelligence,* **PAMI 6**, 6, 661-674.

(32) H. Espedal (1999): Detection of oil spill and natural film in the marine environment by spaceborne SAR, Conference proceedings, IGARSS'99, 3, 1478-1480.

(33) A. H. S. Solberg and E. Volden (1997): Incorporation of prior knowledge in automatic classification of oil spills in ERS SAR images, Conference proceedings, IGARSS'97, 1, 157-159.

(34) H. A. Espedal and T. Wahl (1999): Satellite SAR oil spill detection using wind history information, *Int. J. of Remote Sensing,* **20**, 1, 49-65.

(35) H. Assilzadeh, S. B. Mansor (2001): Early warning system for oil spill using SAR images, Conference proceedings, ACRS 2001 - 22nd Asian Conference on Remote Sensing, Singapore, 5-9 November, 1, 460-465.

(36) M. Gade and J. Redondo (1999): Marine pollution in European coastal waters monitored by the ERS-2 SAR: a comprehensive statistical analysis, Conference proceedings, OCEANS'99 MTS/IEEE Riding the Crest into the 21st century, 3, 1239-1243.

(37) J. M. Keller, S. Chen, R. M. Crownover (1989): Texture description and segmentation through fractal geometry, *Computer Vision, Graphics, and Image Processing,* **45**, 150-166.

(38) G. Benelli and A. Garzelli (1999): Oil-spills detection in SAR images by fractal dimension estimation, Conference proceedings, IGARSS'99, 1, 218-220.

(39) C. R. Jackson, and J. R. Apel (editors) (2004): Synthetic Aperture Radar Marine User's Manual, U.S. Department of Commerce, National Oceanic and Atmospheric Administration (NOAA).

APPENDIX

A ABBREVIATIONS

CFAR	Constant False Alarm Rate
DoG	Difference of Gaussian
EC	European Commission
ESA	European Space Agency
FCM	Fuzzy C-means algorithm
GLCM	Grey Level Co-occurrence Matrices
HMC	Hidden Markov Chain
KSAT	Kongsberg Satellite Services
LoG	Laplace of Gaussian
MLP	Multiplayer Perceptron
MLZ	German pollution control authorities
NR	Norwegian Computing Center
NRCS	Normalized Radar Cross Section
PRI	Precision Image Mode
SAR	Synthetic Aperture Radar
SYKE	Finnish pollution control authorities
WSM	Wide Swath Mode